OE Optical Engineering

RESEARCH PAPER

Probability density function models for adaptive optical systems operating in turbulence

Larry B. Stotts[a,*] **and Larry C. Andrews**[b]

[a]Resident Consultant, Science and Technology Associates, Arlington, Virginia, United States

[b]University of Central Florida, Towns Laser Institute, College of Optics, Center for Research in Electro-Optics and Lasers, Orlando, Florida, United States

ABSTRACT. This work deals with the effect of adaptive optics (AOs) configuration options, i.e., tip/tilt ($N = 3$) and full AO ($N = 35$) cases, on the intensity probability density functions (PDFs) associated with the turbulent channel. An *ad hoc* scintillation index model is proposed for the full AO options. This model is applicable for both power-in-the-bucket and power-in-the-fiber (PIF) signal receptions. The commonly used log-normal intensity PDF follows the no AO and tip/tilt experimental horizontal link data for two turbulence conditions but fails to accurately characterize the full AO option for those two cases, especially in depicting the perceived left skewness of the PDF in one case. The exponentiated Weibull distribution with the proposed full AO scintillation index model exhibits good agreement with the experimental data in the two cases and follows the strong left skewness in one case. These results also show that the median value for each PDF shifts to the right and the PDFs experience narrower shape changes, i.e., more received power, as AO Zernike modes are added. Finally, comparison of PIF PDF shifts with the estimated fiber coupling efficiencies is in reasonable agreement.

Keywords: free space optical communications; turbulence; fiber coupling

Paper 20240312G received Mar. 29, 2024; revised Jun. 26, 2024; accepted Jul. 22, 2024; published Aug. 13, 2024.

1 Introduction

Free-space optical communications (FSOCs) is becoming an important option for both atmospheric and space-based high data rate networks.[1–4] FSOC links operating in and through the Earth's atmosphere must mitigate the effects of turbulence if they are to provide reliable high link availability under cloud-free atmospheric conditions. Methods with varying degrees of success in mitigating turbulence effects include adaptive optics (AOs), interleaving, forward error correction, optical automatic gain control, hybrid RF/FSOC system operation, and networking.[5–10] Validated statistical models for quantifying the effects of turbulence on various FSOC link configurations are available.[11–13]

This paper deals with the effect of AO configuration options, i.e., tip/tilt ($N = 3$) and full AO ($N \sim 35$) on the intensity probability density functions (PDFs) associated with the weak turbulent channel or short-range links under daytime operation.[9,10,14,15] Comparisons will be made between theoretical predictions and daytime experimental field data. An *ad hoc* scintillation index model is proposed for the full AO option. The commonly used log normal (LN) PDF follows the no AO and tip/tilt options but fail to accurately characterize the full AO option. This option is better matched to the exponentiated Weibull (EW) distribution to cover its left skewness nature.[11]

*Address all correspondence to Larry B. Stotts, lstotts@stassociates.com

This new model is applicable to both power-in-the-bucket (PIB) and power-in-the-fiber (PIF) signal receptions as will be shown. In addition, comparison of PIF PDF shifts with the estimated fiber coupling efficiencies are in reasonable agreement.

2 Probability Density Function for the Turbulence Channel

The ultimate performance of an FSOC system operating in and through the Earth's atmosphere is derived by averaging the key performance parameter like bit error rate with respect to the turbulence-induced intensity PDF. This calculation yields the average performance parameter for the assumed turbulence conditions. The validated FSOC in turbulence models used in this paper are described in Ref. 13. Arguably, the two most used turbulence-induced PDFs are the LN and Gamma–Gamma (GG) PDFs. Two exceptions are the use of the modulated Gamma PDF and Gamma PDF in calculations involving untracked-beam and tracked-beam satellite communications uplinks, respectively.[13]

The LN PDF is given as

$$p_{\ln I}(I') = \frac{1}{I'\sqrt{2\pi\sigma^2_{\ln I}(D_{rx})}} \exp\left\{-\frac{[\ln(I') + 0.5\,\sigma^2_{\ln I}(D_{rx})]^2}{2\sigma^2_{\ln I}(D_{rx})}\right\}, \tag{1}$$

with $\sigma^2_{\ln I}(D_{rx}) = \ln[1 + \sigma^2_I(D_{rx})]$, which is valid in the weak-to-moderate intensity fluctuations regimes when the receiver aperture is large [Ref. 12, p. 94]. In this equation, $I' = I/\langle I(0,R)\rangle$ is the normalized received intensity, I is the intensity at the receiver aperture, $\langle I(0,R)\rangle$is the average intensity at the receiver aperture, R is the range, $\sigma^2_I(D_{rx})$ is the aperture-averaged power scintillation index (flux variance), and D_{rx} is the receiver aperture diameter.

The other PDF is the GG PDF, which is written as

$$p_{\mathrm{GG}}(I') = \frac{2(\alpha\beta)^{(\alpha+\beta)/2}}{\Gamma(\alpha)\Gamma(\beta)} (I')^{(\alpha+\beta)/2-1} K_{\alpha-\beta}(2\sqrt{\alpha\beta I'}), \tag{2}$$

where $K_\nu(x)$ is the modified Bessel function of the second kind

$$\alpha = 1/\sigma^2_X(D_{rx}), \tag{3}$$

and

$$\beta = 1/\sigma^2_Y(D_{rx}), \tag{4}$$

with $\sigma^2_X(D_{rx})$ being the large-scale power scintillation index and $\sigma^2_Y(D_{rx})$ being the small-scale power scintillation index [Ref. 12, p. 94].

Equation (2) is valid in the weak-to-strong intensity fluctuations regimes when the receiver aperture is small as well as with certain large values of D_{rx}. Experimental and computer simulation results indicate that Eq. (2) may be only valid in deep turbulence when $D_{rx} < \rho_0$ or when $D_{rx} > R/k\rho_0$with $\rho_0 = r_0/2.1$ being the lateral spatial coherence radius, $k = 2\pi/\lambda$, r_0 is Fried parameter, and λ is the laser wavelength. For apertures sizes between these extremes, the Eq. (1) may be the better model [Ref. 12, p. 94].

3 Experimental Data Collection

Researchers from AOptix operated a 10.02 km FSO link between Campbell, California, United States and Saratoga, California, United States on July 23, 2008 and August 27, 2008, respectively.[9,10] Figure 1 shows a Google-Earth view of the link and its terrain cross-section. The altitudes of the end points are 200 feet at the Campbell site and 1842 feet at the Saratoga site. The slant angle is 2.9 deg in free air but is much closer to ground as the terrain slowly rises into the Santa Cruz Mountains. As you might expect, the turbulence is quite variable and has a strong diurnal cycle, often dominated by local effects at the Campbell site in the day and the interface of the cool marine layer at or below 2000 feet to the upper atmosphere. For this analysis, we will assume this is a horizontal link close to the ground.

For the cited experiments, the FSO link used the AOptix Open frame R3.1 optical terminals of 10 cm aperture, and the same type of optical terminal used in the Hawaii link described in Ref. 7. Figure 2 shows a picture of the AOptix adaptive optical R3.1 optical terminal,

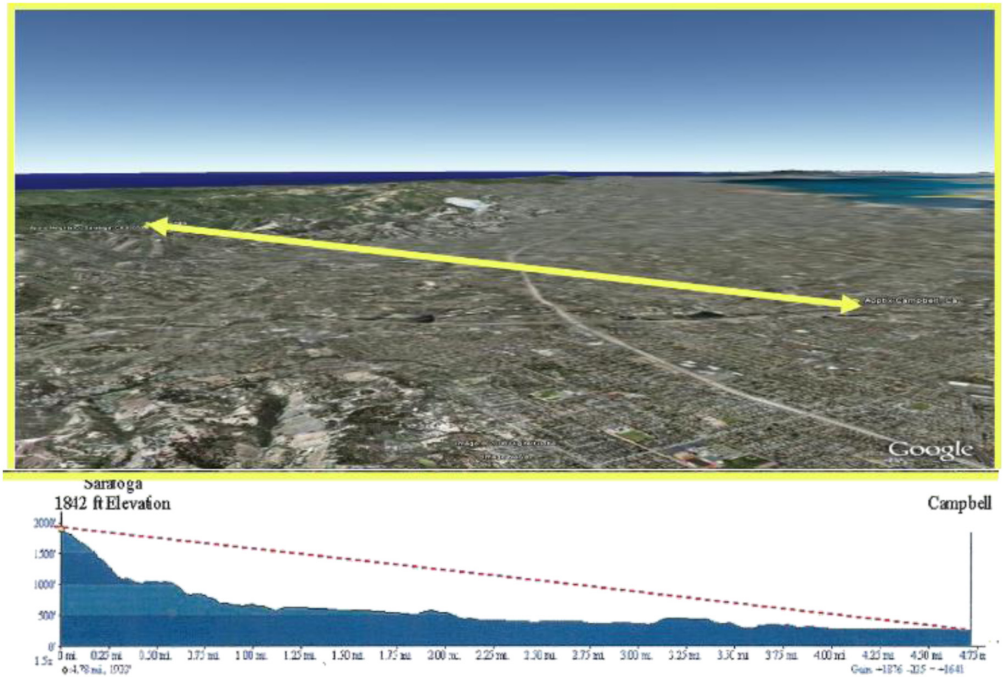

Fig. 1 Google-Earth view of the FSO link and its terrain cross-section.

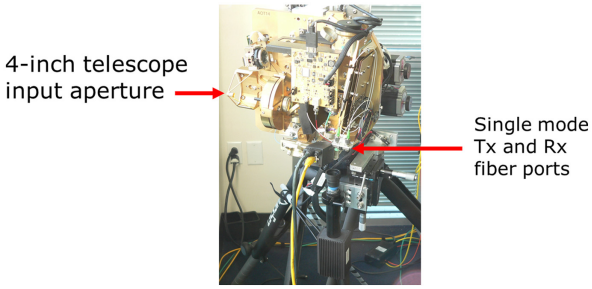

Fig. 2 Picture of the AOptix adaptive optical R3.1 optical terminal.

highlighting the telescope entrance aperture and transmitter and receiver fiber port. AO compensation reduces the severity of the atmospheric effects by reducing phase aberrations induced by the turbulence to increase the amount of power focused into the fiber. The R3.1 AO design incorporated three modes of operations: (1) no AO, (2) tip/tilt only (N.3) and (3) 35-Zernike mode phase correction (N.35). The deformable mirror was driven by 35 actuators in "curvature sensor" architecture for the phase variations detected by the wavefront sensor. The sampling and correction was designed to be well within the Greenwood time interval of the turbulence [Ref. 12, p. 75], which is a measure of how rapidly the atmosphere changes. Figure 3 illustrates the first 10 Zernike modes and some of the aberrations that mode is intended to correct.[15]

Figure 4 depicts a simplified layout of this terminal. The laser wavelength was 1.55 μm. The experiments' data collections involved collecting PIF and PIB measurements at a 32 kHz sample rate, with 1-s statistics generated every minute. High-speed focal plane 64×64 images were taken at 350 frames/s with an exposure time of 0.4 ms and 128×128 images were also taken at 100 frames/s with an exposure time of 1.5 ms.

At this point, we need to define two key parameters, PIB and PIF. Referring to Fig. 4, the total power on the AO wave front sensor is referred to as the PIB. It is a reasonable facsimile of the total power entering the telescope aperture. The power at the single mode fiber entrance aperture is referred to simply as the PIF, as shown in Fig. 4. It is a reasonably accurate, but scaled, facsimile of the Strehl ratio, i.e., it shows how close we get to the Airy disk

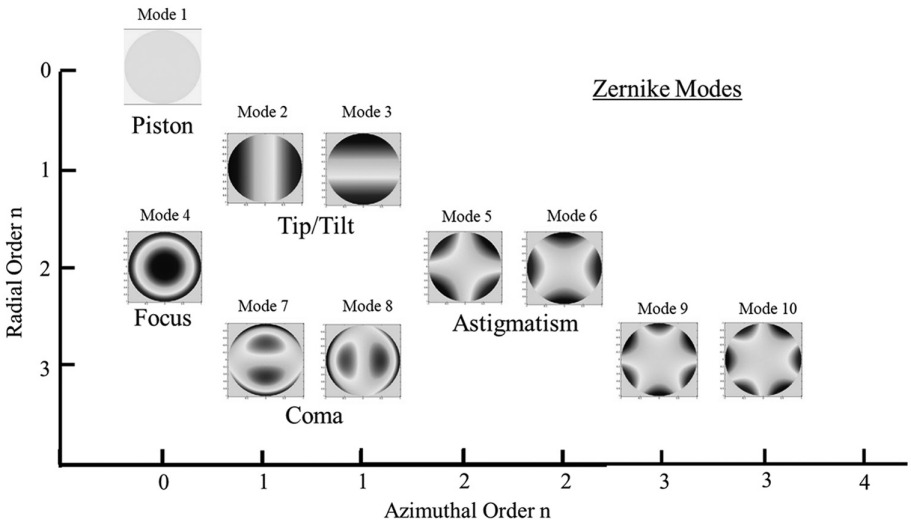

Fig. 3 The first 10 Zernike modes.

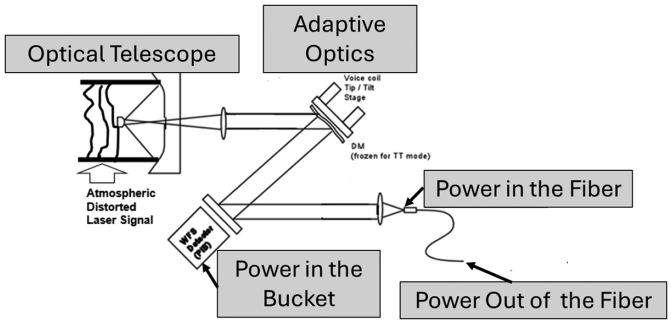

Fig. 4 Simplified layout of the AOptix Open frame R3.1 optical terminals.

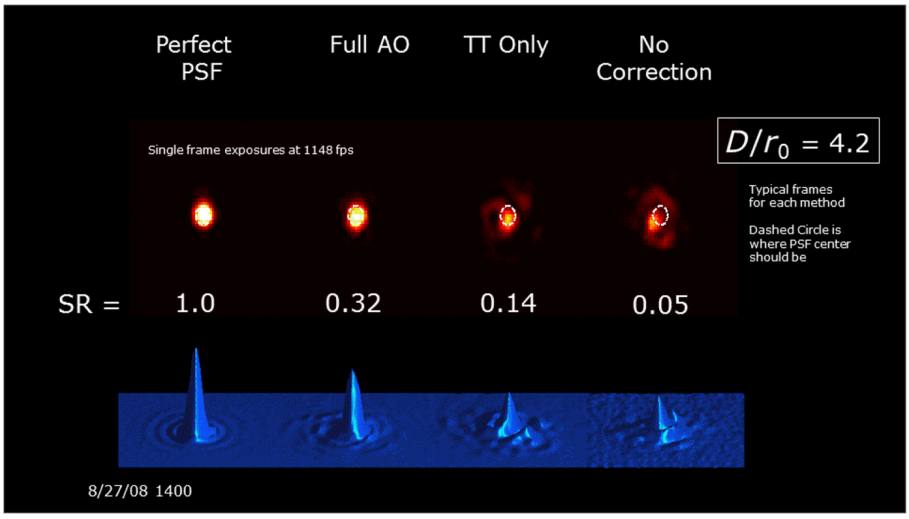

Fig. 5 AO-corrected PSF after turbulence degradation as compared to a perfect PSF.[14]

[Ref. 12, p. 78]. Figure 5 shows the resulting point spread function (PSF) reconstruction and Strehl ratio for data taken at 1400 local time on August 27, 2008, under high intensity fluctuation turbulent conditions. Even with 35-Zernike mode compensation, the AO system could not reconstruct the PSF perfectly. This figure also illustrates that without tip/tilt (TT) beam wander compensation, the focused beam could not center the incoming beam onto the fiber

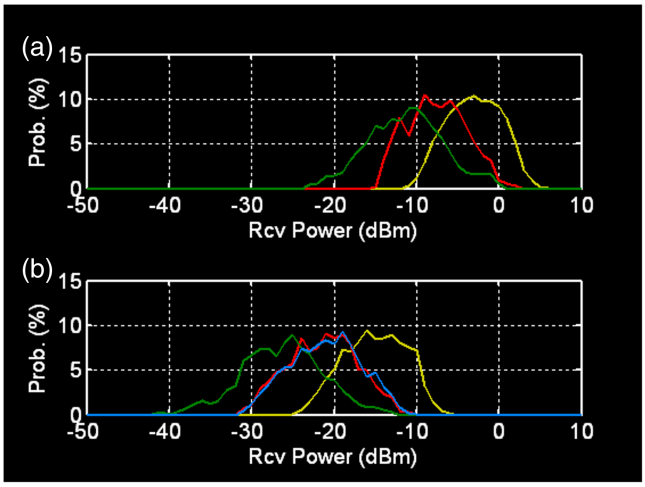

Fig. 6 Focal plane derived (a) PIB and (b) PIF measurements taken at 1400 on August 27, 2008.

aperture. The power exiting the single mode fiber is referred to simply as the power out of the fiber.

Figures 6(a) and 6(b) show focal plane derived PIB and PIF measurements, respectively, taken at 1400 local time on August 27, 2008. The 1400 data collection was taken under $D_{rx}/r_0 = 4.25$ turbulent conditions. The green curves represents PIB and PIF measurements without the AO systems at the two ends of the link working, the red curves depicts the PIB and PIF measurements with the tip/tilt only option of both AO systems being on, and the yellow curves exhibit the PIB and PIF measurements with the 35-Zernike Mode AO system operating at both ends. The blue curves in Fig. 6(b) represent the PIF measurement using the instantaneous frame-by-frame TT correction. This graph clearly shows limited benefit from the use of a higher TT bandwidth. They also show that the median value for each PDF shifts to the right, i.e., improved link performance, as AO Zernike modes are added. In addition, the PDF shapes change similarly. This is not too surprising as one would expect the AO system would increase received power by centering the energy profile along the fiber core axis and reducing spot size and angular spread of the received signal.

Figures 7(a) and 7(b) show PIB and PIF measurements, respectively, taken at 0900 local time on August 27, 2008. The 0900 data collection was taken under $D_{rx}/r_0 = 2.1$ turbulent conditions. The color-coding definitions for both figures are the same as in Fig. 6.

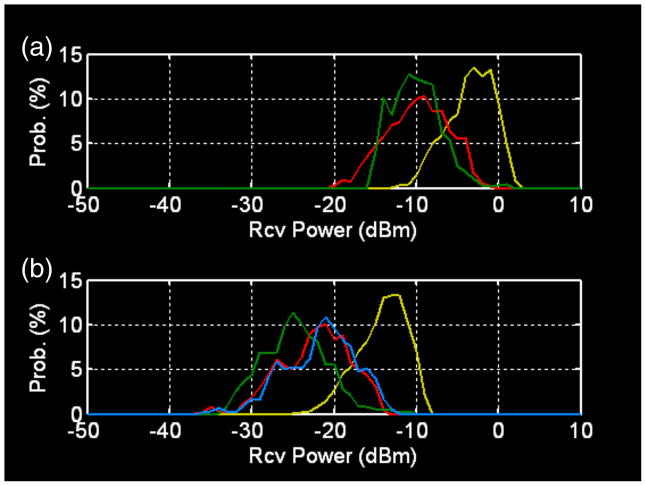

Fig. 7 Focal plane derived (a) PIB and (b) PIF measurements taken at 0900 on August 27, 2008.

4 Horizontal Link PDF Comparison Analysis

The validated FSOC in turbulence models presented below are from Ref. 13. The beam wander variance and pointing error variance in the detector plane for the assumed horizontal link are written as

$$\langle r_c^2(D_{Rx})\rangle = \frac{2.42C_n^2R^3}{W_0^{1/3}}\left(\frac{\Omega_{Rx}}{\Lambda_1+\Omega_{Rx}}\right), \tag{5}$$

and

$$\sigma_{pe}^2(D_{Rx}) = \frac{2.42C_n^2(h_{tx})R^3}{W_0^{1/3}}\left(\frac{\Omega_{Rx}}{\Lambda+\Omega_{Rx}}\right)\left[1-\left(\frac{\pi^2W_0^2/25r_0^2}{1+\pi^2W_0^2/25r_0^2}\right)^{1/6}\right], \tag{6}$$

respectively with $\Omega_{Rx} = 2R/kW_{Rx}^2$ and $W_{Rx} = D_{rx}/2\sqrt{2}$.

The Rytov variance, long-term beam radius, and short-term beam radius in the pupil plane are given as

$$\sigma_R^2 = 1.23C_n^2(h_{tx})k_0^{7/6}R^{11/6}, \tag{7}$$

$$W_{\mathrm{LT}} = W(1+1.33\sigma_R^2\Lambda^{5/6})^{3/5}, \tag{8}$$

and

$$W_{\mathrm{ST}} = \sqrt{W_{LT}^2 - \langle r_c^2\rangle}. \tag{9}$$

The wander-induced power scintillation index in the detector plane is equal to

$$\sigma_{I,\mathrm{Untracked}}^2(D_{Rx}) = 4.42\frac{\sigma_R^2\Lambda_{\mathrm{ST}}^{5/6}\sigma_{pe}^2}{W_{\mathrm{ST}}^2} + \exp[\sigma_{\ln X}^2(D_{Rx},l_0) - \sigma_{\ln X}^2(D_{Rx},l_0,L_0) + \sigma_{\ln Y}^2(D_{Rx})] - 1, \tag{10}$$

and the tip/tilt-tracked power scintillation index in the detector plane equals

$$\sigma_{I,\mathrm{Tip-Tilt}}^2 = \exp[\sigma_{\ln X}^2(D_{Rx},l_0) - \sigma_{\ln X}^2(D_{Rx},l_0,L_0) + \sigma_{\ln Y}^2(D_{Rx})] - 1, \tag{11}$$

with l_0 is the inner scale of the turbulence, L_0 is the outer scale of the turbulence, and $\Lambda_{\mathrm{ST}} = 2R/k_0W_{\mathrm{ST}}^2$. Specific equations for the parameters $\sigma_{\ln X}^2(D_{Rx},l_0)$,$\sigma_{\ln X}^2(D_{Rx},l_0,L_0)$, and $\sigma_{\ln Y}^2(D_{Rx})$ are found in Refs. 12 and 13.

Let us now address the scintillation index for a full AO system. Roddier modified the wavefront variance model to account for the number of mirror actuators

$$\sigma_{wf}^2(N) = 0.335\ N^{-5/6}\left(\frac{D_{rx}}{r_0}\right)^{5/3}, \tag{12}$$

where N is the number of mirror actuators.[16] The reduction in wavefront variance between $N = 3$ and $N = 35$ AO systems equals

$$\Delta\sigma_{wf}^2 = \frac{\sigma_{wf}^2(N=35)}{\sigma_{wf}^2(N=3)} = \left(\frac{35}{3}\right)^{-5/6} = 0.129. \tag{13}$$

If we assume that this reduction applies directly to the scintillation index reduction with increasing Zernike modes, then the tracked power scintillation index is reduced by 0.129, i.e.

$$\sigma_{I,\mathrm{FullAO}}^2 = 0.129\sigma_{I,\mathrm{Tip-Tilt}}^2. \tag{14}$$

Figure 8 compares the LN PDFs for no AO, tip/tilt, and full AO options using the above equations against their associated PIB measurement curves shown in Figs. 3(a) and 4(a). The no AO and tip/tilt comparisons in Fig. 8(a) are in reasonable agreement, but the full AO comparison is not good. The LN curve is much narrower than the measurement curve. The tip/tilt comparisons in Fig. 8(b) are in reasonable agreement, although slightly shifted, but the no AO and full AO comparisons are not good. The full AO LN curve is much narrower than and not left skewed like the measurement curve. The left-hand side of no AO LN curve is broader than the left-hand

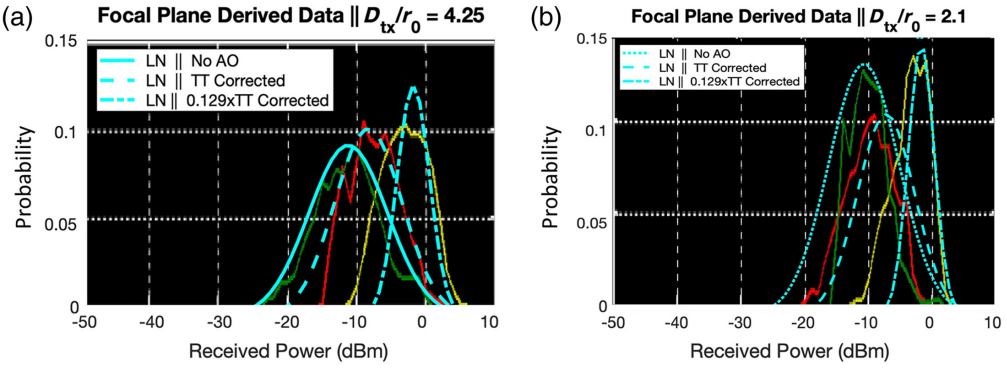

Fig. 8 Comparison of LN PDFs and PIB data taken at (a) 1400 and at (b) 0900 on August 27, 2008.

side than measurement curve. The right-hand sides are closer, but the LN curve is broader here as well. Since we are interested in the AO options performance, we will not worry about this difference.

Looking at Fig. 8(b), we see a left skew that neither an LN nor GG PDF can create by any combination of parameters.[11] Barrios and Dios suggested that a different PDF should be used when aperture averaging takes place and found that an EW distribution agreed with both simulation and experimental data.[17] It also creates a left skew PDF profile. This distribution is given as

$$p_{\mathrm{ew}}(I') = [\eta\alpha/\beta](I'/\beta)^{\alpha-1} e^{-(I'/\beta)^{\alpha}} [1 - e^{-(I'/\beta)^{\alpha}}]^{\eta-1}, \tag{15}$$

where the shape parameter η obeys the following approximation

$$\eta = 3.931 \left(\frac{D_{rx}}{\rho_0}\right)^{-0.519}, \tag{16}$$

the shape parameter α' is given as

$$\alpha' = (\eta\, \sigma_I^2(D_{rx}))^{-6/11}, \tag{17}$$

the scale parameter β' equals

$$\beta' = \frac{1}{\eta\, \Gamma(1 + 1/\alpha') g(\eta, \alpha')}, \tag{18}$$

and

$$g(\alpha', \eta) = \sum_{n=0}^{\infty} \frac{(-1)^n\, (n+1)^{(1+\alpha')/\alpha'} \Gamma(\eta)}{n!\, \Gamma(\eta - 1)}. \tag{19}$$

Figure 9 compares the LN PDFs with the no AO and tip/tilt PIB data, and the EW PDF using the above equations with the full AO PIB data found in Figs. 6(a) and 7(a). There is no change in our observation of the no AO and tip/tilt comparisons from Fig. 8. However, we now see that the EW curves agree reasonably well with PIB measurements in both figures. In fact, the EW curve exhibits the left skew seen in full AO data curve shown Fig. 9(b). This suggests that the EW distribution represents the full AO situation much better than the LN or GG distributions could. This comparison also shows that the full AO option reduces the PDF width as compared to the no AO and tip/tilt (TT) cases.

Looking at the PIF curves in Figs. 6(b) and 7(b), the shapes of these PDFs appear to be like those shown in Figs. 6(a) and 7(a) but just shift down about 13 dB. We noted earlier that the PIF was the power at the fiber face in the experimental setup.

Figure 10 compares shifted LN PDFs with the no AO and tip/tilt PIF data, and shifted EW PDF with the full AO PIF data found in Figs. 6(b) and 7(b). The curves appear to agree quite well. The shifts in Fig. 10(a) are −15, −12.5, and −11.5 dB for no AO, TT only, and full AO configurations, respectively. The shifts in Fig. 10(b) are −15, −15, and −12 dB for no AO, TT only, and full AO configurations, respectively. Figure 11 exhibits the PDF for the fiber coupling efficiency (EFC) for the (a) 1400 and (b) 0900 experiments normalized by the receiver system loss of

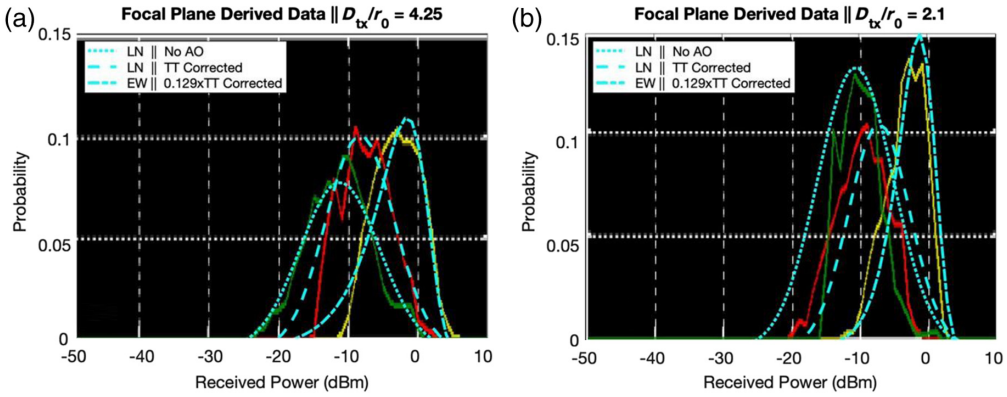

Fig. 9 Comparison of LN PDFs for no AO and tip/tilt A0 and EW PDF for full AO and PIB Data taken at (a) 1400 and at (b) 0900 on August 27, 2008.

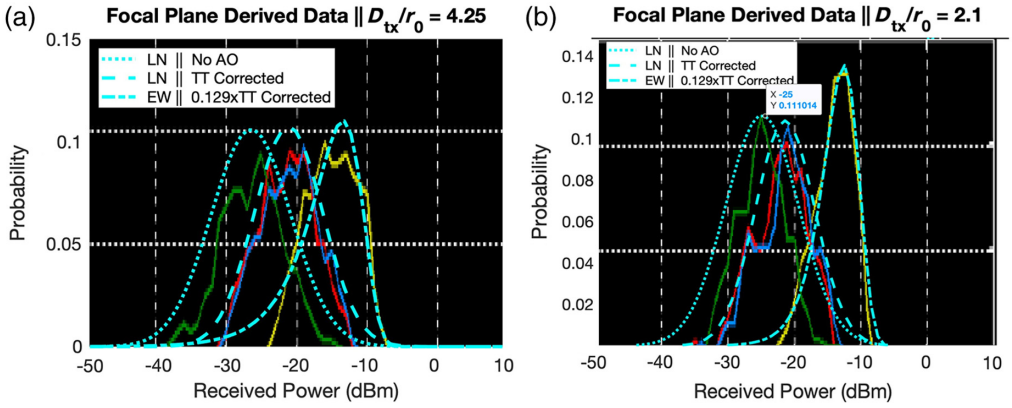

Fig. 10 Comparison of LN PDFs for no AO and tip/tilt A0 and EW PDF for full AO and PIF data taken at (a) 1400 and at (b) 0900 on August 27, 2008.

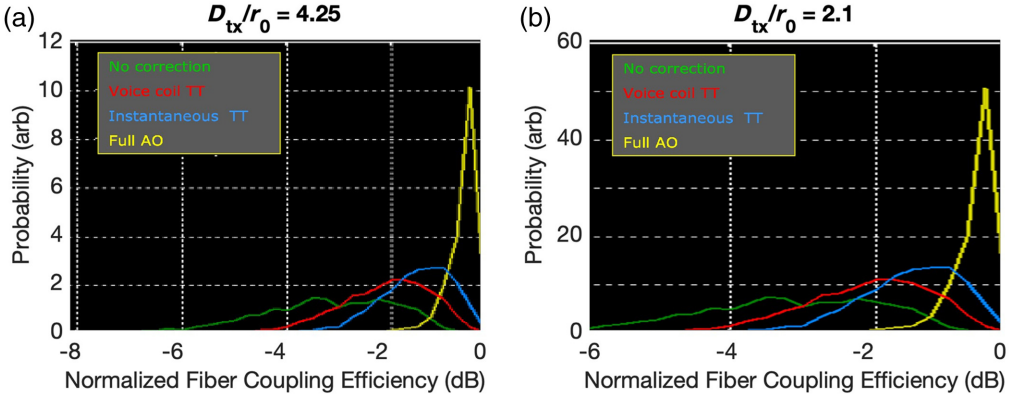

Fig. 11 Normalized fiber coupling efficient PDF measured at (a) 1400 and at (b) 0900 on August 27, 2008.

10 dB.[9] Table 1 compares the above shifts to the eye-ball estimated EFCs for the (a) 1400 and (b) 0900 experiments. They are in reasonable agreement. Let us look in more detail at the results depicted in Fig. 10.

The mean values appear consistent with the TT Only and full AO PDFs for both Figs. 10(a) and 10(b). The PDF shape agreement between the TT only predictions and full AO estimates, and the experimental measurements are also reasonably good.

Table 1 Comparison of PDF shift for Fig. 10 with the estimated fiber coupling efficiencies.

8.27.2008 0900	Image shift (dB)	Estimated normalized EFC (dB)	EFC (dB)
No AO	−15	−3	−13
TT only	−15	−2	−12
Full AO	−12	−0.8	−10.8
8.27.2008 1400	Image shift (dB)	Estimated normalized EFC (dB)	Estimated normalized EFC (dB)
No AO	−15	−5	−15
TT only	−12.5	−3.5	−13.5
Full AO	−11.5	−1.8	−11.8

On the other hand, the no AO PDF and data comparisons show the PDF profile centered about right but depict much narrower shape profiles than the theoretical predictions do. The PDF peak value is quite different from the mean value. This suggests that the no AO PDF model does not characterize the received intensity statistics correctly when the received signals are coupled into fibers. This additional loss may be attributed to beam wander causing many signals not to be coupled into the fiber. The other two situations are effectively centroid tracked by the $N = 3$ portion of the AO system, which minimizes the beam wander-induced fiber coupling losses. In any event, most optical communications systems will employ an AO system for at least tracking purposes and the above estimates suggest a benefit in link performance by their use as compared to their non-use in weak turbulence or short range.

5 Summary

This paper dealt with the effect of AO configuration options, i.e., tip/tilt ($N = 3$) and full AO ($N \sim 35$), on the intensity PDF associated with the weak turbulent channel or short-range links under daytime operation. Comparisons will be made between theoretical predictions and experimental field data. This paper showed that the LN PDF can be used as no AO and tip/tilt ($N = 3$) turbulence-induced intensity PIB and PIF PDFs but does not represent the full AO ($N = 35$) PDF very well. The better PIB and PIF PDF option for full AO is the EW PDF that both match the profile and the left skewness that results from its use. These results also showed that the median value for each PDF shifts to the right and the PDFs experience narrower shape changes, i.e., more received power, as AO Zernike modes are added. In addition, PIF PDF shifts and the EFCs were shown to be in reasonable agreement.

Disclosures

No conflict of interest.

Code and Data Availability

Data underlying the results presented in this paper are not publicly available, as AOptix, the company that took the data, no longer exists.

Acknowledgments

The authors would like to acknowledge and thank Mr. Buzz Graves, Dr. Dave Daugherty, and Mr. Jeff Douglas, all formerly of AOptix, for taking the data shown in the above figures. The Defense Advanced Research Projects Agency (DARPA) has approved this paper for unlimited distribution (Distribution A). The views, opinions, and/or findings contained in this article are those of the authors and should not be interpreted as representing the official views or policies, either expressed or implied, of the DARPA, or of the Department of Defense.

References

1. C. Chen et al., "Demonstration of a bidirectional coherent air-to-ground optical link," *Proc. SPIE* **10524**, 105240G (2018).
2. H. Kaushal and G. Kaddoum, "Optical communication in space: challenges and mitigation techniques," *IEEE Commun. Surv. Tutor.* **19**(1), 57–96 (2017).
3. A. Mansour, R. Mesleh, and M. Abaza, "New challenges in wireless and free space optical communications," *Opt. Lasers Eng.* **89**, 95–108 (2017).
4. S. Seel et al., "Space to ground bidirectional optical communications link at 5.6 Gbps and EDRS connectivity outlook," in *Aerosp. Conf.*, Big Sky, Montana, pp. 1–7 (2011).
5. L. B. Stotts and L. C. Andrews, "An adaptive optics model characterizing turbulence mitigation for free space optical communications link budgets," *Opt. Express* **29**(13), 20307–20321 (2021).
6. L. B. Stotts et al., "Hybrid optical RF communications," *Proc. IEEE* **97**(6), 1109–1127 (2009).
7. C. Zachary et al., "Hybrid optical radio frequency airborne communications," *Opt. Eng.* **51**, 055006 (2012).
8. J. C. Juarez et al., "Analysis of link performance for the FOENEX laser communications system," *Proc. SPIE* **8380**, 838007 (2012).
9. J. E. Graves, D. Daugherty, and J. Douglas, DARPA Optical RF Communications Adjunct (ORCA) Program, private communications.
10. L. B. Stotts et al., "Free space optical communications link budget estimation," *Appl. Opt.* **49**(28), 5333–5343 (2010).
11. L. C. Andrews and M. K. Beason, Chap. 5 in *Laser Beam Propagation through Random Media: New and Advanced Topics*, SPIE Press, Bellingham, Washington (2023).
12. L. C. Andrews, *Field Guide to Atmospheric Optics*, 2nd ed., SPIE Press, Bellingham, Washington (2019).
13. L. B. Stotts and L. C. Andrews, "Optical communications in turbulence: a tutorial," *Opt. Eng.* **63**(4), 041207 (2024).
14. S. Karp and L. B. Stotts, "Visible/infrared imaging on the rise," *IEEE Digital Signal Process. Mag.* **30**(6), 178–182 (2013).
15. S. Karp and L. B. Stotts, Chap. 10 in *Fundamentals of Electro-Optic Systems Design: Communications, Lidar, and Imaging*, Sect. 10.5, Cambridge Press, New York (2013).
16. F. Roddier, "Maximum gain and efficiency of adaptive optics systems," *Publ. Astron. Soc. Pac.* **110**, 837–840 (1998).
17. R. Barrios and F. Dios, "Exponentiated Weibull distribution family under aperture averaging for Gaussian Beam waves," *Opt. Exp.* **20**(12), 13055–13064 (2012).

Larry B. Stotts is a consultant. His interest areas are RF and optical communications, and RF, infrared and visible surveillance, and reconnaissance. He received his BA degree in applied physics and information sciences and PhD in electrical engineering (communications systems), both from the University of California at San Diego. He has published over 115 journal articles and authored/co-authored four books. He is a fellow of IEEE, SPIE, and Optica.

Larry C. Andrews is a Professor Emeritus of mathematics at the University of Central Florida (UCF) and an associate member of the Towns Laser Institute in the College of Optics/CREOL at UCF. He received his PhD in theoretical mechanics from Michigan State University. He has authored/coauthored 12 textbooks and has published numerous papers and reports. He is a fellow of SPIE and authored three SPIE field guides.